Polar-step Driven Metal Nucleation and Growth: The Ag/ZnO(1010) Case

Stefania Benedetti, Ilaria Valenti, Sergio Valeri, Sebastián Castilla, Edouard Touzé, Yael Bronstein, Alexandra Toumar, Fabio R.D. Finocchi, Rémi Lazzari

HAL Id: hal-02878555

https://hal.sorbonne-universite.fr/hal-02878555v1

Submitted on 23 Jun 2020

Polar-step Driven Metal Nucleation and Growth: The Ag/ZnO$(10\bar{1}0)$ Case

Stefania Benedetti,*,† Ilaria Valenti,‡ Sergio Valeri,‡ Sebastián Castilla,¶ Edouard Touzé,¶ Yael Bronstein,§ Alexandra Toumar,§ Fabio Finocchi,¶ and Rémi Lazzari*,¶

†CNR-Istituto Nanoscienze, via Campi 213/a 41125 Modena, Italy
‡Dipartimento di Scienze Fisiche Informatiche Matematiche, Università di Modena e Reggio Emilia and CNR-Istituto Nanoscienze, via Campi 213/a 41125 Modena, Italy
¶CNRS, Sorbonne Université, Institut des NanoSciences de Paris, UMR 7588, 4 Place Jussieu, F-75005 Paris, France
§Saint-Gobain Recherche, 39 quai Lucien Lefranc, 93303 Aubervilliers, France

E-mail: stefania.benedetti@nano.cnr.it; remi.lazzari@insp.jussieu.fr

Abstract

The morphology, epitaxy, band-alignment and optical response of silver nanoparticles on ZnO$(10\bar{1}0)$ has been analysed by microscopy, photoemission, electron diffraction and differential reflectivity. At 700 K, clusters tend to nucleate and grow exclusively along [010]-oriented polar steps and corners, and not on flat terraces or non-polar [001] steps. This preference leads to a specific epitaxy Ag(111)[1$\bar{1}$0] ∥ ZnO[010]$(10\bar{1}0)$ with a large lattice mismatch along the dense row of the metal. The experiments have been rationalized through *ab initio* simulations. A much lower adsorption energy is obtained for the O-terminated steps with a charge transfer from silver to oxygen, that corroborates the variation of ionization energy observed in photoemission and the presence of cationic silver. This anisotropy of growth reverberates in the plasmonic response of the metallic particles. The growth and epitaxy of metals on the polar (0001) and non-polar $(10\bar{1}0)$ orientations of ZnO is discussed in terms of surface/step polarity compensation in the light of the present findings.

Introduction

Encapsulated in complex stack of films, silver layers are widely used by the glass industry as the active element for infrared reflection in low-emissive or anti-solar coatings.[1,2] Their mechanical resistance and ability to withstand dewetting upon annealing during windows tempering or shaping rely on the metal adhesion at the interfaces. Among the potential oxide substrates, ZnO wurtzite turned out to be one of the best candidates in terms of silver wetting. Beyond the argument of a reduced band-gap compared to bulk-insulating oxides[3] and of a good cristallization during sputtering deposition, several fundamental reasons have been put forward to explain the enhanced adhesion on ZnO.[4]

The first argument relies on the polarity of the (0001) orientation in the wurtzite structure[5] since the polycrystalline ZnO layers on which silver is deposited display a strong c-axis fibre texture. Among different mechanisms such as creation of vacancies or hydroxylation, charge transfer to the deposited metal should allow to circumvent the polar catastrophe *i.e.* the electrostatic divergence of the surface potential due to the alternate stack-

ing of Zn cation and O anion planes along the [001] direction.[6,7] The adhesion energy between Ag and the ideal, bulk-like ZnO(0001)-Zn and (000$\bar{1}$)-O terminations was computed to be rather high.[8] However, several mechanisms are at work to make the existing surfaces already polar-compensated before metal growth, which actually deeply modifies their atomic and electronic structures and lower the adhesion with the Ag overlayer. The actual mechanisms are still debated and they depend on the specific surface termination (either Zn or O) and chemical environment; for instance, surface hydrogen load and departure from the ideal stoichiometry are quite entangled.[9-19]

A good metal adhesion on an oxide substrate is often due to epitaxy and lattice matching between the two systems. In this respect, the case of Ag/ZnO(0001) is quite puzzling. Previous grazing incidence X-ray diffraction measurements[20,21] on vapour-deposited Ag on ZnO single crystals showed that the metal adopts on both faces, Zn and O-terminated, a so-called hexagon/hexagon Ag[1$\bar{1}$0](111) $\parallel$ ZnO[100](0001) orientation with a lattice mismatch of -11 % despite an expected lower value (-3.8 %) for the 30°-rotated orientation. This finding was assigned to a perfect coincidence of (9×9) unit cells of Ag every (8×8) surface unit cells of ZnO. Nevertheless, growing nanoparticles (NPs) that require a size of at least 2.6 nm to feel this coincidence were found stress-free at their bulk lattice parameter for coverage above half a monolayer. In parallel, small-angle X-ray scattering evidenced a quasi-2D growth and a good apparent wetting; flat-top and high-aspect ratio (diameter/height) (111)-oriented NPs cover rapidly the whole surface. Similar findings in terms of epitaxial orientation and bidimensional growth morphology were also obtained for other face centred cubic metals such as Cu,[22-25] Pd[26] or Pt.[27,28] ZnO precipitates in Ag matrix share also the hexagon/hexagon orientation.[29] But according to simulations, the hexagon/hexagon orientation is slightly more stable than the rotated one.[8]

The morphology, epitaxy and stress state of Ag NPs on the polar faces of ZnO run counter classical expectations about metal/oxide growth. As previously shown for Ag/Al$_2$O$_3$(0001)[30] or Ag/MgO(001),[31] beyond an undoubtful non-wetting 3D growth of low aspect ratio particles, the NPs lattice parameter is driven by the interplay between surface and interface stresses.[32] Below a critical size of about 3 nm, a contraction or expansion is observed depending on the sign of the metal/oxide misfit, while above this size the strain state obeys the "Laplace pressure" law. Such an unusual behaviour of Ag/ZnO(0001) NPs could be due to the large density of defects, in particular step edges, that exist on the polar faces of ZnO. Indeed, for vacuum annealed ZnO(0001)-Zn, a dense array of triangular pits and holes is observed by scanning tunneling microscopy,[10,33] which, according to atomistic simulations,[10,11,19] are non-stoichiometric and provide the required charge to heal the surface polarity. Noteworthy, the ZnO nanostructures exhibit [100]-oriented edges that are terminated by rows of O or Zn ions and are themselves polar. The morphology of the ZnO(000$\bar{1}$)-O-termination is less clear-cut and the actual mechanism of the surface polarity compensation is still debated, although the saturation of half the O surface anions with protons is likely in the experimental conditions.[17] As far as a metal growth is concerned, a likely explanation is a step-induced nucleation and quick lateral growth of the NPs with the alignment of the dense rows along the step edge.[34] The copper NPs growth clearly goes with a charge transfer as determined by the evolution of band-bending and work function.[22,23] Silver is cationic (anionic) on ZnO(000$\bar{1}$)-O (ZnO(0001)-Zn) at low coverage, before adsorbing as a neutral species when the particle size increases and eventually form a Schottky barrier.[35] Whether the charge transfer originates from healing the step or the surface polarity, and how it reinforces the metal-oxide chemical bonding remains anyway unclear.

In order to understand the role of the step edges on metal adsorption, the non-polar ZnO(10$\bar{1}$0) orientation is a better playground

than ZnO(0001)-Zn and ZnO(000$\bar{1}$)-O owing to the complexity of polarity compensation on the latter terminations. The ZnO(10$\bar{1}$0) surface is characterized by the presence of rectangular holes and pits with perpendicular steps of different terminations[36–38] (Figure 1). While [001] steps expose compensated facets made of equal numbers of cations and anions, [010] steps are polar, either O or Zn terminated.[6,7] The specific role of steps was already underlined in the case of Cu/ZnO(10$\bar{1}$0)[19,39] or Cu/ZnO(0001)-Zn.[25,34,40,41]
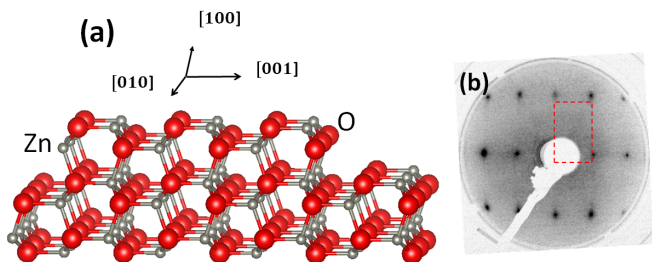

Figure 1: (a) Atomic ball model of the ZnO(10$\bar{1}$0) surface with oxygen anions in red and zinc cations in grey. Steps running along the [010] direction are either O- or Zn-terminated while perpendicular ones along the [001] direction are composed equally of both ions. Main directions are indicated by arrows. (b) LEED pattern of a ZnO(10$\bar{1}$0) clean surface ($E_B = 120$ eV) with its rectangular unit cell ((5.207 × 3.25) Å²).

Nucleation, epitaxy and band-alignment have been probed during Ag growth on ZnO(10$\bar{1}$0) by a combination of Scanning Tunneling Microscopy (STM), Low-Energy Electron Diffraction (LEED) and Ultra-violet Photoemission Spectroscopy (UPS). The impact of the surface anisotropy and of the charge transfer on the plasmon resonances in the NPs was also explored at macroscopic scale by UV-visible polarized Surface Differential Reflectivity Spectroscopy (SDRS). Beyond shape and density anisotropies,[42,43] charging upon contact with the support and size reduction[44] may influence plasmon resonances and de-excitation mechanisms,[45–47] with influences on the charge dynamics,[48] like in the case of the material catalytic response.[49] Experiments haves been supplemented herein by *ab initio* simulations in the framework of the Density Functional Theory (DFT) to analyse the formation energies of the various step terminations as well as the preferred Ag adsorption site and its charge state.

Methods

Experiments

Experiments were conducted into two separated vacuum vessels (Modena/Paris) with base pressures in the low 10^{-10} mbar and both equipped with X-ray photoemission spectroscopy (XPS) and LEED facilities. ZnO(10$\bar{1}$0) single crystal surface (provided by SurfaceNet) was prepared by cycles of sputtering and annealing at 1100 K until reaching a satisfactory LEED pattern (Figure 1-b) and the lack of contaminants at the sensitivity of XPS. Silver was deposited from a temperature regulated thermal evaporation cell at a base pressure in the high 10^{-10} mbar and keeping the substrate either at 300 or 700 K. The evaporation rate around 1 Å/min was previously calibrated *in situ* with a quartz microbalance.

A hemispherical analyzer (EA125 Omicron) working at normal emission and at constant pass energy was used (i) for XPS measurements under Al-Kα non-monochromatic X-ray excitation and (ii) for UPS under He I excitation (at an overall resolution of 0.1 eV). Binding energy scale was set on the Fermi level of a clean Ag reference crystal. The work function of metal deposit on ZnO was measured from the secondary electron cutoff by polarizing the sample at -20 V to reaccelerate the low energy electrons. Samples were conductive enough to prevent any noticeable charge effects with all the above cited techniques. STM images were collected on an Omicron RT UHV AFM/STM with a chemically etched W tip. Images were analyzed by means of WSxM[50] and SPIP softwares.

The growth process of silver was followed in real-time by SDRS at an incident angle of 55°. The experimental setup (previously described in Ref. 51) allowed recording simultaneously the s- and p-polarization states of light. The incident plane was aligned parallel or perpendicular to the [001] surface direction of ZnO($10\bar{1}0$) to within a few degrees through electron diffraction. The back face of the substrate was tarnished to avoid back reflection. Shortly, SDRS consists in recording the relative variation of the sample reflectivity in the UV-visible range (1.5-4.5 eV) by using the bare substrate signal as a reference. The incoming light excites localized surface plasmon absorption modes[51–53] in the growing NPs, which position and intensities are highly sensitive to the morphology and to the electromagnetic interaction with the substrate and among the collections of NPs.[51,52] Associated to dielectric modellings,[54–59] this optical technique already allowed to describe growth nucleation, growth and coalescence processes of supported NPs and their shape evolution.[30–32,60] In s-polarization, the electric field being parallel to the surface can only excite modes parallel to the surface. Since the electric field is in the plane of incidence in p-polarization, both parallel and perpendicular active modes can be excited. Silver being a test bed for plasmonics, submonolyer sensitivity could be easily achieved owing to the contrast of dielectric function with the substrate and of the excitation of very intense plasmon resonances.

Ab initio simulations

DFT calculations have been carried out by means of the Quantum Espresso suite,[61] within the Generalized Gradient Approximation (GGA),[62] in conjunction with the use of ultra-soft pseudo-potentials. Systematic tests showed that the convergence of the total energy, atomic forces and crystal parameters can be attained at 50 Ryd cutoff energy on the plane-wave basis set. The computed values of the lattice constants a = 3.283 Å (3.25 Å), c = 5.296 Å (5.207 Å) slightly overestimate the experimental ones (in brackets)) as usual in GGA; the parameter defining the relative position of O with respect to Zn along the [001] axis is $u = 0.379$.

The ZnO($10\bar{1}0$) surfaces were simulated through slabs of variable thicknesses, consisting of M ($10\bar{1}0$) double layers, with $4 \leq M \leq 12$, and a void space that is as thick as 12 planes. The surface Brillouin zone was sampled by a (5×3) grid, centred at Γ point. The slab total energy $E(M)$ can be written as the sum of the surface contribution and the bulk one as:

$$E(M) = 2A_0\sigma_0 + ME_{bulk}, \qquad (1)$$

where A_0 and σ_0 are the ZnO($10\bar{1}0$) surface area and energy, respectively, and E_{bulk} the energy of the crystalline bulk.[63] From the previous formula, by means of a linear regression, both bulk and surface energies are obtained. After extensive checks, the computational set-up ensures the convergence of the surface energy within 0.03 J/m^2 $\simeq$ 2 meV/Å^2.

Vicinal surfaces with ($10\bar{1}0$) terraces and steps oriented along either [010] (polar) or [001] (non-polar) were simulated through shifted periodic boundary conditions.[64] The energy for the formation of step per unit of length λ_θ can be written as the difference between the surface energies of the vicinal and the flat surfaces as:

$$a\lambda_\theta = A_\theta\sigma_\theta - A_0\sigma_0, \qquad (2)$$

where θ is the angle between the vicinal surface $\mathbf{n_\theta}$ and flat surface $\mathbf{n_0}$ normal directions, A_θ and σ_θ the vicinal surface area and energy, respectively, and a the lattice parameter along the step direction. In all slab calculations, the atoms in the two innermost layers were kept fixed in their ideal bulk positions, whereas all the others were free to relax, until the atomic forces reduced to less than 2 meV/Å. By simulating several terrace widths (*i.e.* various θ), the step energy was found via a linear regression.

Different kinds of step were simulated: (i) the non-polar step, parallel to [001], and (ii) two polar steps, either type-A or type-B (Figure 5). The resulting step energies vary between 0.10 eV/Å (for non-polar [001] steps) to 1.06 eV/Å

4

(for type-A polar [010] steps) and 0.42 eV/Å (for type-B polar [010] steps). This hierarchy of energies matches with the trends observed by STM of step elongation along the non-polar [001] direction upon annealing at high temperatures.[65] As the actual termination of the steps on ZnO(10$\bar{1}$0) are unknown from the experiments, we systematically simulated distinct edges and studied the first stages of Ag adsorption, on different sites, in order to determine the most relevant stable adsorption configurations in thermodynamic equilibrium conditions.

Results and discussion

Nucleation and epitaxy

When Ag is deposited on ZnO(10$\bar{1}$0) surface at room temperature, no clear-cut extra spots are observed in the LEED pattern. After annealing at 900 K, extra features help assigning the Ag[1$\bar{1}$0](111) ∥ ZnO[010](10$\bar{1}$0) epitaxial orientation (Figure 3). The 2.89 Å hexagonal unit
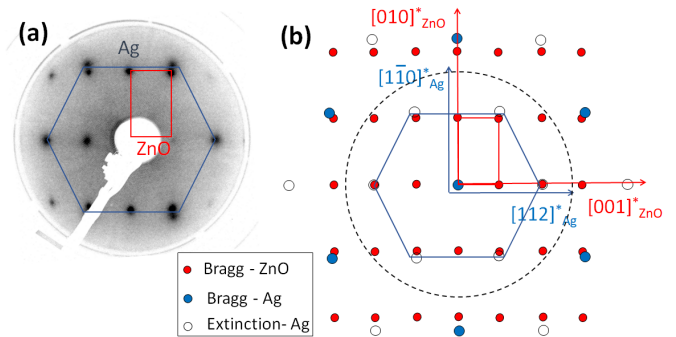
Figure 3: (a) LEED pattern ($E_B = 140$ eV) of a 20 Å deposit of Ag/ZnO(10$\bar{1}$0) after annealing at 900 K and (b) scheme of the reciprocal space of bulk Ag(111) and ZnO(10$\bar{1}$0). Red (respectively blue) disks correspond to ZnO (respectively Ag) bulk Bragg diffraction while open circles stand for bulk extinction in Ag that may be active in LEED. Dotted line stand for the LEED field of view.

cell of Ag(111) surface has -3.8 % and -10.9 % lattice mismatches along the [001] and [010] directions of ZnO(10$\bar{1}$0), respectively. This last figure runs counter classical expectation of
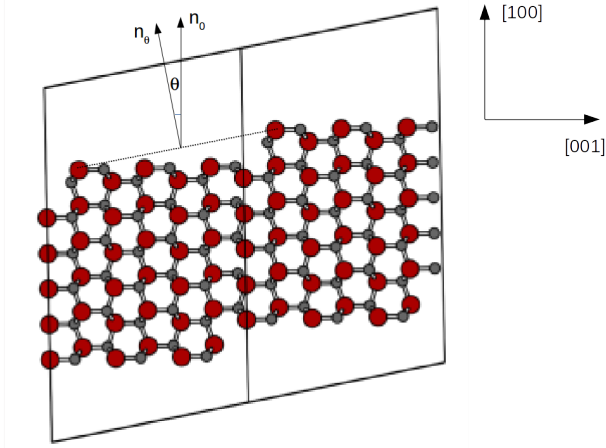

Figure 2: Ball model of a slab model of ZnO vicinal surface with O (red) and Zn (gray). The slab consists here of 6 double ZnO(10$\bar{1}$0) layers and the steps run along the [010] direction, with step length equal to a. The step height $h = a$ corresponds to a ZnO double layer and the terrace width to $L = 2.5c$, where a and c are the computed ZnO lattice parameters. $\mathbf{n}_\theta$ and $\mathbf{n_0}$ are the normal directions to the vicinal surface and the (10$\bar{1}$0) terraces, respectively, and θ the angle of the vicinal surface as adopted in Equation 2. Shifted periodic boundary conditions are made apparent by the representation of two supercells along the shifted direction.

5

minimal mismatch in epitaxial relationship. Interestingly, the alignment of the dense rows of Ag along the [010] direction of ZnO was already observed in the case of the Ag(111) epitaxy on ZnO(0001)-Zn and ZnO(000$\bar{1}$)-O polar orientations.[20,21] As [010]-oriented steps are present on all these surfaces,[10] the specific alignment of dense rows of Ag along the common [010] direction despite a high mismatch could be explained by a [010] polar step-driven nucleation and growth.

In order to confirm the role of steps at the onset of Ag growth, a local analysis by STM was performed. According to images (Figure 4), the ZnO(10$\bar{1}$0) surface is characterized by flat terraces limited by atomic [010] polar and [001] non-polar steps. A zoom at high resolution on
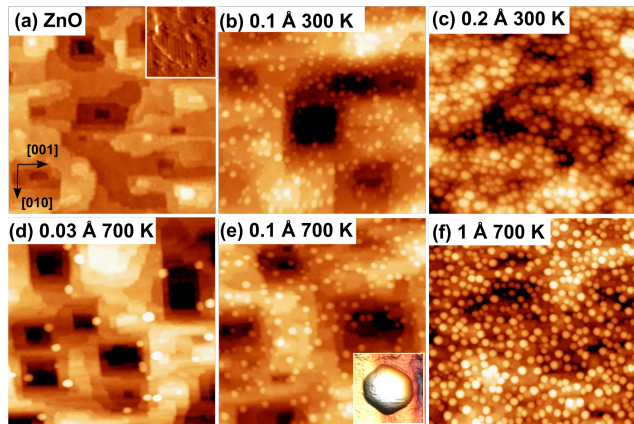

Figure 4: (100×100 nm^2) STM images of (a) bare ZnO(10$\bar{1}$0) surface with (b) 0.1 Å and, (c) 0.2 Å Ag deposited at 300 K, (d) 0.03 Å, (e) 0.1 Å, (f) 1 Å Ag deposited at 700 K ($U = 2.5$ V, $I = 0.04$ nA). Inset of (a) shows a high resolution (8×6.6) nm^2 zoom of the ZnO terraces; the zoom (e) on a Ag NP (10×10) nm^2 shows its hexagonal shape.

a terrace (inset Figure 4-a) confirms the alignment of step edges with atomic rows separated by $\simeq 5$ Å, as previously reported for this surface.[37] The apparent step height is found close to a multiple of $h \simeq 3.3$ Å, which corresponds to the bulk periodicity of ZnO bilayers perpendicular to the (10$\bar{1}$0) plane, with a preference for a single bilayer.

When Ag is deposited on this surface, it spontaneously nucleates in the form of NPs. Apparent lateral size, height and density of the NPs obtained from STM grain analysis are reported in Tab. 1. Like for Cu/ZnO(10$\bar{1}$0),[39] the growth is clearly 3D since, at the early beginning, NPs have an height of 3-4 atomic planes. The hexagonal prismatic shape shown in the inset of Figure 4-e, with its tips aligned along the [010] direction of ZnO agrees with the epitaxy relationship found in LEED. But no clear shape anisotropy induced by nucleation and growth along the step edges was observed. The morphology strongly depends on the deposition temperature as confirmed by SDRS lineshapes (see below). When NPs are formed at 300 K, their apparent lateral size is between 2.5 and 4 nm and reaches an apparent complete coverage of the surface well below 1 Å if tip convolution is not accounted for. At 300 K, preferential nucleation occurs at step edges but some NPs appear randomly distributed all over the terraces as well. But when the growth temperature is raised up to 700 K, the NPs increase in size and their density is reduced as expected from thermally enhanced diffusion. Astonishingly, they nucleate exclusively on corners or on polar [010] borders; excluding coner sites, a slight preference for one termination (0.65 : 0.35, Figure 4-d) is observed assuming an alternance of Zn and O step termination from one terrace to the other. But neither apparent step height nor width statistics allow a clear assignment of the favored termination.

The experimental difficulty in determining the specific step termination (either O or Zn) and the precise Ag adsorption sites motivated us to run several first-principle simulations, with distinct substrate configurations: (i) the flat surface, (ii) the non-polar [001] step, (iii) the polar [010] step, either O- or Zn-terminated. For each substrate configuration, several likely non-equivalent adsorption sites for Ag atoms have been considered, in the limit of almost isolated adatoms or full Ag rows. The Ag adsorption enthalpy was computed through the difference of the computed total energies between the surface with adatom(s), on the one

Table 1: Ag nanoparticle morphology as obtained from STM image analysis. Thickness is estimated from quartz microbalance assuming a sticking coefficient of one. Quantities are not corrected from tip convolution.

Temperature (K)	Nominal thickness (Å)	Particle density ($\times 10^{12}$ cm^{-2})	Apparent coverage (%)	Apparent diameter (nm)	Apparent height (nm)	Aspect ratio (d/h)
300	0.1	2.4	12	2.5	1	2.5
300	0.2	5.6	90	4.0	1.5	2.7
700	0.1	2.0	12	2.85	1	2.8
700	0.2	2.4	20	3.0	0.8	3.7
700	0.5	1.6	30	3.7	1.5	2.5
700	1	3.6	50	3.2	1.6	2.0

side, and the clean surface plus the Ag dimer, on the other side: $\Delta H_{\mathrm{ad}} = E(\mathrm{Ag:ZnO}) - E(\mathrm{ZnO}) - E(\mathrm{Ag}_2)/2$. The dimer has been chosen as the reference system for silver, mainly for two reasons: Ag_2 is an "intermediate" system between the isolated atom and the bulk, very likely present in the experimental deposition by evaporation; moreover, the adsorption enthalpy can be directly compared to the case of hydrogen, where the molecule H_2 is the reference system.

Firstly, let's focus on the adsorption of an isolated Ag atom. To that aim, a Ag atom per (3×3) surface supercell is considered, with Ag-Ag shortest distance between periodic images equal to $3a \simeq 9.85$ Å. The adsorption enthalpy ΔH_{ad} for selected configurations did not vary significantly when considering larger 2D supercells. On the flat $\mathrm{ZnO}(10\bar{1}0)$ terraces, there are two preferential adsorption sites, the bridge (BR) and hollow (HL) ones (see Figure 5). The BR site is more stable than the HL, with $\Delta H_{\mathrm{ad}} = -0.28$ eV/atom. In the BR configuration, the Ag binds to O ($d_{\mathrm{Ag-O}} = 2.20$ Å) and Zn ($d_{\mathrm{Ag-Zn}} = 2.74$ Å). On non-polar [001] steps, the preferred adsorption site is the hollow site at the step edge (see Figure 5-b), where Ag binds to two O ($d_{\mathrm{Ag-O^{(s)}}} = 2.35$ Å and $d_{\mathrm{Ag-O^{(t)}}} = 2.40$ Å) and two Zn ($d_{\mathrm{Ag-Zn^{(s)}}} = 2.95$ Å and $d_{\mathrm{Ag-Zn^{(t)}}} = 2.80$ Å) [1]. For comparison, the bond lengths that are obtained by summing the ionic radii R_{ion} and the co-

(a) Terrace — $\Delta H_{\mathrm{ad}} = -0.28$ eV

(b) Step [001] — $\Delta H_{\mathrm{ad}} = -0.48$ eV

(c) Step [010]-Zn — $\Delta H_{\mathrm{ad}} = -0.95$ eV

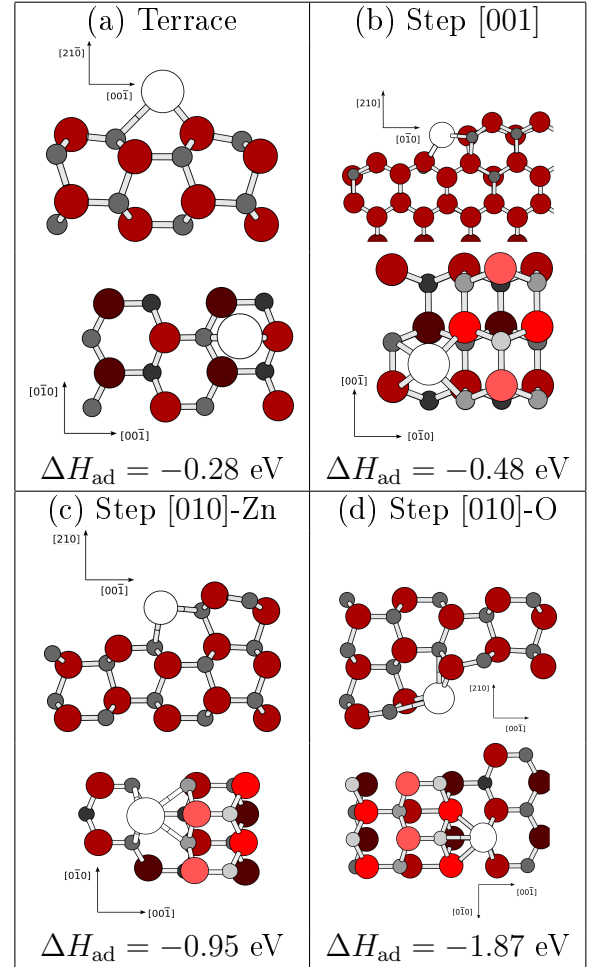(d) Step [010]-O — $\Delta H_{\mathrm{ad}} = -1.87$ eV

Figure 5: Synoptic of the preferred adsorption sites for a Ag adatom on $\mathrm{ZnO}(10\bar{1}0)$ (flat surface and with steps). In the sketch of the adsorption configurations, white, red and grey balls stand for Ag, O and Zn atoms, respectively; the darker, the deeper into the bulk from the topmost layer. For each configuration, the corresponding adsorption enthalpy ΔH_{ad} per Ag adatom is reported.

---

[1]For the sake of clarity, $\mathrm{X^{(t)}}$ and $\mathrm{X^{(s)}}$ denote atoms of type X at terraces and step edge, respectively

valent radii R_{cov} are: $R_{ion}(O^{2-}) + R_{ion}(Ag^+) =$ 2.55 Å and $R_{cov}(Ag) + R_{cov}(Zn) = 2.84$ Å. The corresponding adsorption enthalpy is $\Delta H_{ad} = -0.48$ eV/atom, thus about double compared to the flat terrace. The adsorption strength is enhanced on [010] polar steps. On the Zn-terminated step, the HL site is favoured, with $\Delta H_{ad} = -0.95$ eV/atom; Ag binds to 4 Zn, two on the step edge and two on the terrace ($d_{Ag-Zn^{(s)}} = 2.74$ Å, $d_{Ag-Zn^{(t)}} = 2.76$ Å). Overall, the preferred adsorption site for an isolated Ag is the HL site at the O-terminated [010] polar step, with $\Delta H_{ad} = -1.87$ eV, thus slightly more stable than the BR site ($\Delta H_{ad} = -1.69$ eV) at the same step. In the HL site, Ag binds to four O, two on the edge and two on the terrace, forming also two loose bonds with Zn. It is worth noting that the adsorption enthalpy of Ag at the O-terminated [010] polar step, for both HL and BR sites, is more negative that its counterpart for hydrogen ($\Delta H_{ad} = -1.4$ eV/H atom); in contrast with the polar ZnO$(000\bar{1})$-O surface, silver adsorption is favoured over protonation. This has important consequences, as the onset of Ag adsorption at [010]-O steps on the ZnO$(10\bar{1}0)$ surface could be practically unaffected by the presence of residual hydrogen in the deposition chamber.

If the deposition is done at thermodynamic equilibrium, the isolated Ag atoms are preferentially adsorbed at the O-terminated [010] polar step, on the hollow sites. This is no longer the case of the Ag$_2$ dimer, which still adsorbs parallel to the O-terminated [010] polar step, but on the two bridge sites. The adsorption of a full, epitaxial Ag row along the step edge was simulated by using a (3×1) surface cell, with a periodically repeated Ag atom at distinct sites close to the step edge. Noteworthy, the dimer adsorption configuration is very similar to the most stable one for an entire Ag row along the O-terminated [010] step, apart from a smaller Ag-Ag distance (2.92 Å in Ag$_2$ instead of 3.28 Å in the case of epitaxial Ag row). Numerical calculations show two trends when considering the the number of Ag adatoms on the stepped ZnO$(10\bar{1}0)$ surface. First, two isolated Ag adatoms are more stable than the Ag$_2$ dimer at the [010] steps (see Figure 6). ΔH_{ad}

increases with the number of Ag up to the completion of a Ag row along the [010] step (where $|\Delta H_{ad}|$ is lower by roughly 20-30% than for the isolated Ag adatom) for the most stable configurations. The relative weakening of the adsorption strength with step coverage can be ascribed to the charged state of the adatoms close to the step, which results into the mutual electrostatic repulsion between themselves. Secondly, according to our simulations, the adsorption of Ag on the O-terminated [010] step is preferred to that on the Zn-terminated edge, whatever the step coverage. This is agreement with the experimental STM images (Figure 4), which show that the nucleation at polar step edges is not uniform, although the step termination could not be determined experimentally.
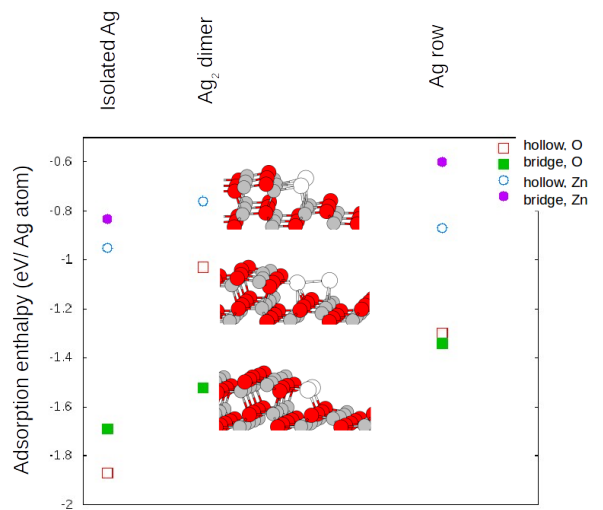

Figure 6: Computed adsorption enthalpies for Ag atoms at polar [010] steps on the ZnO$(10\bar{1}0)$ surface. For the Ag$_2$ dimer, three local minima are shown: (i) the most stable BR-BR configuration, parallel to [010]-O; (ii) the HL-HL configuration, normal to [010]-O; (iii) the HL-HL configuration, parallel to [010]-Zn. Red, green and light gray balls stand for O, Zn and Ag atoms.

From the comparison of the computed ΔH_{ad} for the isolated Ag, the dimer and the entire row, one can conclude that the nucleation on hollow and bridge sites on O-terminated [010]

steps are preferred if Ag is deposited mainly from gas-phase atoms. However, another question could arise: given a Ag adsorbed at O-terminated step edges, where does a second Ag atom go? By comparing the adsorption energies of a Ag_2 dimer at the step and of two Ag adatoms, the first at the O-terminated [010] step and the second in another site, it appears that at the very first stage of Ag deposition, the nucleation on distinct sites is favoured over the growth of a Ag row at the step edges. This could explain the observed lack of anisotropy of particle shape, such as elongation along the step edge. As the density of Ag adatoms at O-terminated [010] steps increases, there could be a competition between the adsorption of a second Ag atom along the O-terminated [010] step forming a dimer and the adsorption at Zn-terminated [010] steps. Clearly, this picture depends on the deposition conditions and kinetics. However, the simulations indicate that the nucleation on multiple sites appears to be favoured onto the sudden growth of Ag rows on few nucleation sites. This picture is consistent with the STM observations (Figure 4).

Charge transfer

The preferential nucleation on step edges can induce noticeable modifications in the electronic properties and the dielectric response of the NPs. They were scrutinized by UPS and SDRS respectively. Up to 1 Å, valence band (VB) spectra (Figure 7-a) are characterized by a Zn 3d derived state feature at around 10 eV and a O 2p/Zn 4s one between 2 and 6 eV. Above this film thickness value, the modifications observed above 4 eV can be assigned to the appearance of Ag 4d derived states. In parallel, the density of states rises up close the Fermi level due to the developement of the Ag 5s metallic character of the clusters. The clear Fermi energy step in the NPs at a thickness of 10 Å validates *a posteriori* the calibration of binding energy scale. The lack of the Ag 5s derived states below 1 Å is not related to a non-metallic/metallic transition of the NPs but more likely due to final state effects in small clusters in which the poor screening

of the hole shifts upward the binding energy.[35] The interpretation is supported by the presence of plasmon resonances, *i.e.* collective oscillations of the electronic cloud coupled to the incident field, in SDRS (Figure 10). since the early stages of the growth. Oscillations on the 10 Å curve of Figure 7 remind the photoemissions observation made in the case of Ag growth on polar faces of ZnO[35] or on ZnO(01$\bar{1}$0)[66] and are assigned similarly to confined Ag 3d states in the NPs.
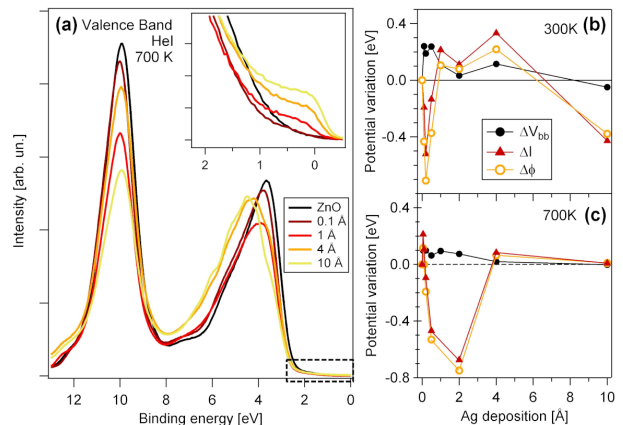

Figure 7: (a) UPS valence band spectra; the inset shows a zoom at the Fermi level. (b,c) Variations of band bending, work function and ionization energy as a function of Ag film thickness for depositions at (b) 300 K and (c) 700 K.

The position of the VB edge was obtained as the crossing point between the linear fit of the flank of the valence band and the background level. From this value, the shift of the VB edge, namely the variation of band bending in the oxide ΔV_{bb} was determined (Figure 7-b,c). The corresponding positive variation points at a downward band bending that impacts also the core level positions (not shown). The maximum ΔV_{bb} occurs at about 0.5 Å and goes to zero at 2 Å for NPs grown at 300 K; at 700 K, those onsets are shifted to 1 Å and 4 Å respectively, pointing at a coverage effect. To understand the origin of this evolution, the work function variation $\Delta \Phi$ was also determined from the low-energy cut-off of secondary electron distribution. As a result, the ionization energy

variation was calculated as $\Delta I = \Delta\Phi + \Delta V_{bb}$. All quantities are reported in Figure 7. ΔI is negative in the range 0-2 Å for 300 K deposition, 0-4 Å for 700 K, when the downward band bending is observed. This indicates the presence of a positive surface dipole at the surface, due to a charge transfer between the Ag NPs to the oxide, with a positive end on the metal side. Above in thickness, silver adsorbs as a neutral species. The different ranges at which charge occurs at the two temperatures are related to the different nucleation densities and coverages as observed in STM. Most likely, ΔI and therefore the charge transfer drop to zero when the NPs saturate the steps. Since the dominant charging is positive and the NPs tend to decorate preferentially one type of the two polar borders, a preference to O-terminated borders is more likely as suggested by atomistic simulations.

To pinpoint the amplitude and direction of the charge transfer, electronic density for Ag adatoms adsorbed at step edge has been scrutinized in the simualtions. Since [010] steps are composed by rows of either O or Zn ions, a polarization normal to the step direction should develop. The internal electric field bends the electron bands, until the levels of the non-bonding states on the O and Zn edges overlap. The O states are partially emptied and the Zn ones partially filled, providing the necessary charge compensation.[6,7] The surface is therefore open-shell. Upon Ag adsorption, one can note an electron transfer from the Ag adatom to the O at the step edge (see Figure 8, right panel). In particular, the extended s-like Ag orbital is depleted, mainly towards p-like orbitals on the neighbouring O ions. This allows for the O at the step edge to recover their typical ionic configuration, while Ag is partially ionized and polarity compensated. As a matter of fact, the adsorption of the Ag_2 dimer in the bridge configuration restores the insulating character of the overall system. When Ag is adsorbed at the Zn-terminated [010] step, there is an electron population increase in the step region between the adatom and the neighboring Zn, at the expense of a d-like Ag orbital (see Fig-

ure 8, left panel). This situation corresponds to a metallic-like binding between Ag and Zn. Experimentally, the order of magnitude of the transferred charge can be deduced from a plane-capacitor modelling of the change of ionization energy: $\Delta I = eNp_\perp/\epsilon_0$.[67] N and $p_\perp$ are the surface density of dipoles and their normal component while e, ϵ_0 have their usual meaning. For a $p_\perp$ dipole length given by the step height (see Figure 8-right), a value of ~ 0.05 e/Ag is found.
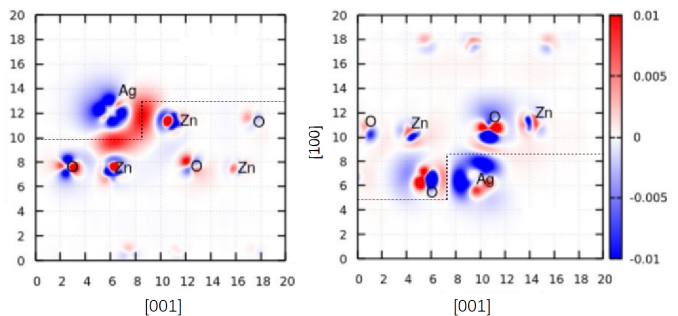

Figure 8: Electron charge density difference after adsorption of Ag rows on bridge sites at Zn-terminated (left) and O-terminated (right) [010] steps. Regions where positive density increases (decreases) after adsorption are plotted in red (blue). The crystal directions are labelled and the step profile sketched by a dashed line.

Anisotropy of the plasmonic response

The anisotropy of Ag nucleation impacts also the optical response of the NPs layer. To highlight this effect, the growth has been followed by differential reflectivity with an incident beam aligned along, either the [010] or the [001] direction. For the sake of clarity, Fig 9 reminds the relative orientations of the electric fields in p- and s-polarization and of the crystallographic directions of Ag/ZnO. Briefly, when the beam is aligned along polar [010] steps, the in-plane electric field component is parallel to the [010] steps in p-polarization and perpendicular to it in s-polarization. This is the reverse when the beam is oriented at 90° along [001] non-polar
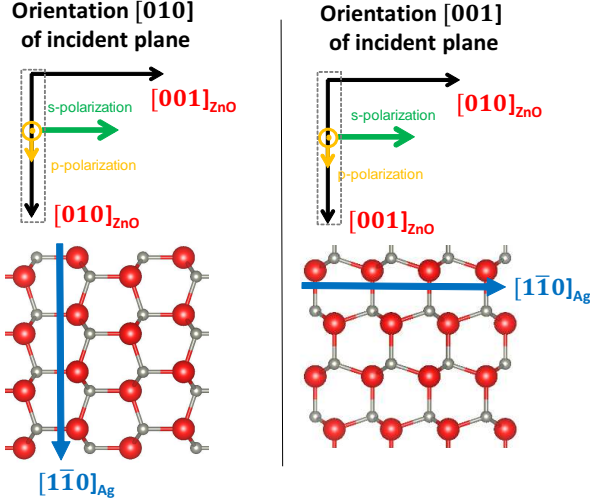
steps. Figure 10 gathers the evolution of SDRS

Figure 9: Relative orientation of the electric fields in s- or p-polarizations and of the crystallographic axis for the two considered beam directions. The dotted grey rectangle stands for the incident plane of light.

signal at 700 K for the two beam directions and the two polarization states in the sub-monolayer regime (Figures 10-a,b) and above (Figures 10-c,d). The spectra are characterized by intense plasmon absorptions in the growing Ag NPs; these are excited by the component of the electric field parallel to the surface (both s- and p-polarizations) for the low energy peak (below 3 eV) and by the normal component (p-polarization only) for the high energy feature (above 3.7 eV). Strikingly, a difference in position of the low-energy resonance between the two polarization states occurs in the sub-monolayer regime (Figures 10-a,c) but vanishes above (Figures 10-b,d). The peak is systematically red-shifted in p-polarization compared to s-polarization for a beam oriented along the [010] polar step edges and vice-versa for the [001] direction. To highlight this effect, the positions of all peaks have been extracted from a parabolic fit of the extremum (Figure 11). The cross-over in position observed between 2-3 Å for the low energy peak between the two polarizations is less clear at room temperature than at 700 K, a finding which is confirmed by a direct inspection of the raw data

of Figure 12 As already shown for Ag NPs on oxides,[31,51,52,56,68,69] the low energy resonance position is an extremely sensitive reporter of morphology; the more red-shifted the flatter or the denser the particles. A less important blue shift is usually found for the high energy resonance with nanoparticle aspect ratio (diameter/height) and particle density. This rule of thumb is fulfilled when comparing peak positions at different growth temperatures (Figure 11) as expected from temperature-induced dewetting. As seen by STM (Fig. 4), no clear anisotropy of shape can put forward to explain the optical anisotropy at the earliest stages of the growth. Moreover, the role of the anisotropy of ZnO bulk dielectric constants can be safely ruled out to explain the present findings on the low-energy plasmon peak. The detailed ellipsometry measurements of Ref. 70 showed that, for a photon energy in the band gap of ZnO where lies the peak of interest, the ordinary and extraordinary directions behave in a similar way. Optical anisotropy of ZnO appears mainly around the exciton absorption close to the band gap edge. At the opposite, the found shift between polarizations for the low energy resonance is compatible with the STM results of denser particles along the polar [010] step edge. Indeed, the dipole-dipole coupling between NPs[51,52,54,71] creates a depolarization field that acts again the parallel plasmon oscillation and therefore red shifts the resonant frequency proportionally to the ratio of the oscillator strength to the spacing between NPs. It is worth noticing that the optical anisotropy disappears at large thickness when, as seen by STM, the surface is covered more randomly by the NPs.

The experimental spectra also show a feature slightly above the 3.2 eV band gap of ZnO (Figures 10,12). Its line shape and position in p-polarization is at odd with an effect of substrate thermoreflectance[72] that could be due to a slight increase of substrate temperature when opening evaporation cell. To see if it matches with the excitation of modes of absorption in Ag NPs,[51–53] SDRS spectra have been inverted using an already discussed Kramers-
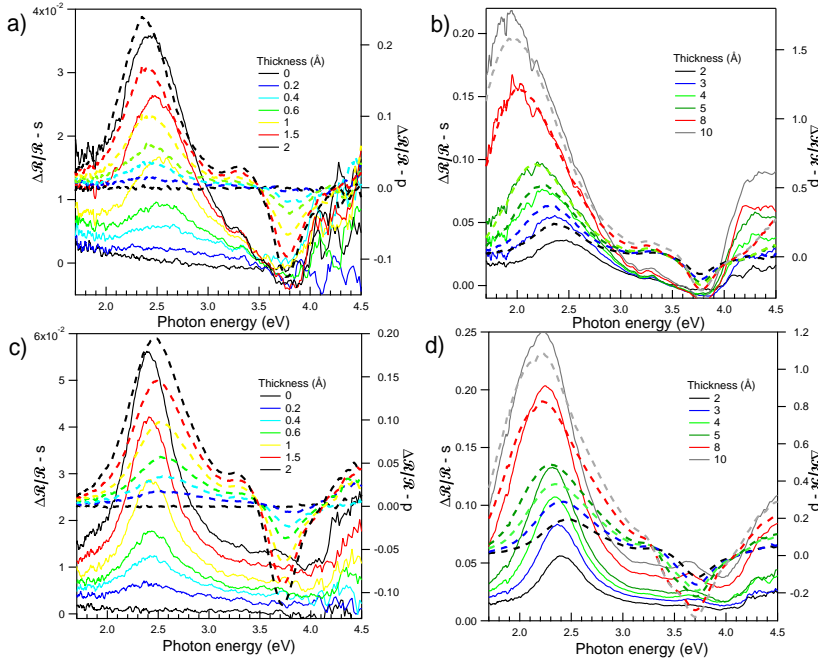
Figure 10: Evolution of SDRS spectra during Ag/ZnO(10$\bar{1}$0) growth at 700 K: beam along (a)(b) [010)]; c)d) [001] (see Figure 9). Dotted lines/right scale (respectively, continuous lines/left scale) correspond to p (respectively, s) polarization. Equivalent film thickness is given in figure.
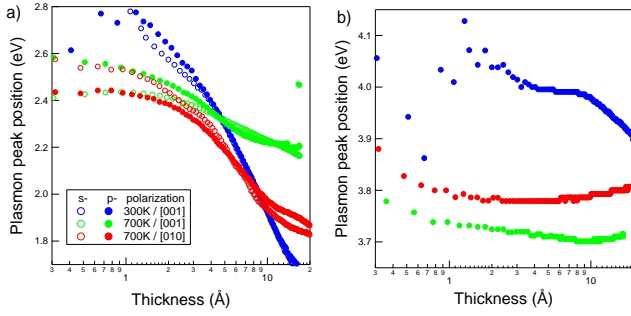

Figure 11: Evolution of (a) low energy and (b) high energy plasmon peak positions. In Figure-(a), s and p signals are compared for various beam orientations and temperatures while only p-polarization is able to probe normal excitation.

Kronig algorithm[51,73] to obtain the interface susceptibilities[54] (IS). These complex dielectric lengths characterize the dielectric behaviour of the film/substrate interface in the direction parallel (γ-IS) and perpendicular (β-IS) to the surface. Shortly, through such a treatment, the dielectric responses of the film alone, parallel and perpendicular to the substrate, are desentangled from the known optical response of the bulk substrate[70] and from the mixture of electric field directions in p-polarization spectra. As seen in the example of Figure 13-a,b, the imaginary part of parallel γ-IS is dominated (i) by an increasing and shifting parallel plasmon resonance[51] below 3 eV and (ii) by the bulk Ag interband transitions above 3.8 eV. Both absorption occurs in the Ag NPs. In fact, as already shown,[51] the experimental plasmon peak encompasses the excitation of dipole-like polarization modes $A_{\parallel}$ and $B_{\parallel}$ in flat particles (see simulation Figure 13-d). But an absorption feature rises between 3.1 and 3.5 eV in the submonolayer regime before saturating at higher thickness at the opposite to the plasmon resonance (see Figure 13-c). Absent from simulations[57,58] with truncated spheroidal particles with bulk dielectric constants,[70,74] it parallels the imaginary part of the bulk dielectric function of ZnO. It is assigned to the modi-
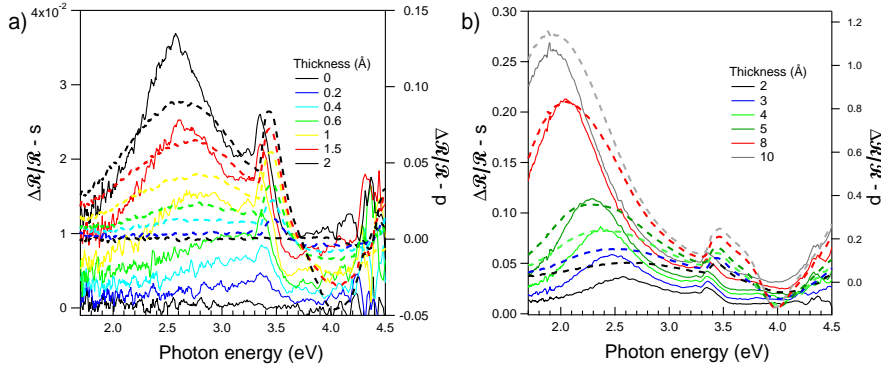
Figure 12: Same as Figure 10 but at a growth temperature of 300 K and for a [001] beam orientation.
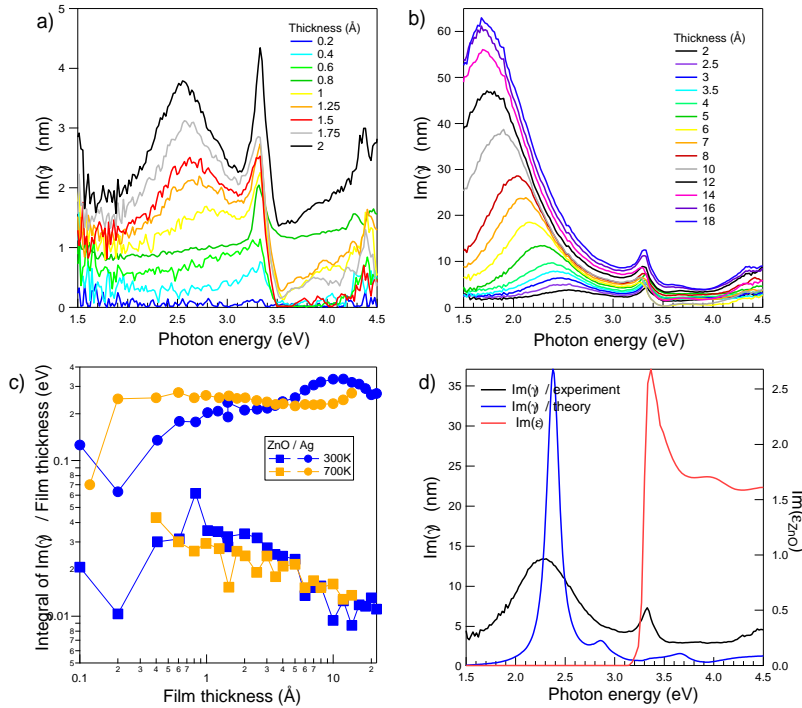

Figure 13: (a)(b) Imaginary part of the interface susceptibility Im(γ) obtained from the inversion of the data of Figure 12. Similar results are obtained at 700 K (not shown). (c) Evolution of Im(γ) integrated over frequency and normalized to the film thickness. Integration is performed in the 1.5-3.15 and 3.15-3.4 eV range for the Ag (squares) and ZnO (circles) signals. (d) A dielectric simulation of Im(γ) for an hemispheroid of Ag on ZnO (blue line) compared to the 5 Å spectrum of Figure 12-b (black line) and to Im(ϵ_{ZnO}), the imaginary part of the bulk dielectric function of ZnO (red line). Note the presence in the simulations of two peaks at 2.35 eV and 2.85 eV corresponding to mode $A_\parallel$ and $B_\parallel$ respectively.

fication of absorption across the band gap of the substrate due to the charge transfer to the bulk. A likely hypothesis is a modulation of the electric field in the ZnO space charge layer that parallels the band bending observed by UPS at the beginning of the growth. The impacted depth as given by the continuous film behaviour of IS[51,54] $\mathrm{Im}(\gamma)/\mathrm{Im}(\epsilon_{ZnO})$ amounts to a few nanometers, an order of magnitude that matches with the Debye length previously determined by photoemission in ZnO crystals prepared by sputter-annealing.[35] The difference of visibility of such a feature in the raw data at 300 and 700 K might be related to a coverage effect of step edge.

Conclusion

The growth of silver on the non-polar ZnO($10\bar{1}0$) surface have been scrutinized by a combination of surface science techniques (LEED, STM, UPS and SDRS) and *ab initio* calculations. If not so clear cut at room-temperature, at 700 K, tridimensional metallic clusters nucleate and growth exclusively at corners and polar [010]-oriented step edges with a preference towards one type of termination. In parallel, the metal aligns its dense row along the same direction despite a large lattice mismatch. According to atomistic simulations, metal adsorption is strongly thermodynamically favoured at step edges compared to flat terrace sites with a strong preference for O-terminated ones. As seen in UPS at the early stages of growth and confirmed by calculations, a charge transfer occurs between the metal and terminal oxygen atoms giving rise to slightly cationic silver and partial healing of step polarity. At the opposite, the binding to Zn-terminated step is more metallic. This anisotropy of nucleation and growth gives rise to an in-plane anisotropic plasmonic response of the clusters. Beyond these resonances, the metal adsorption give rise to a band gap related optical feature that parallels the observed band-bending. This work puts forward the question of polar step healing as a potential

source of apparent good metal spreading and of the astonishing epitaxial relationship of metals at the surfaces of ZnO. Further work is required to tackle the question of the actual impact of the epitaxy on the stress state of the NPs.

References

(1) Jelle, B. J.; Hynd, A.; Gustavsen, A.; Arasteh, D.; Goudey, H.; Hart, R. Fenestration of today and tomorrow: A state-of-the-art review and future research opportunities. *Sol. Energy Mater. Sol. Cells* **2012**, *96*, 1 – 28.

(2) Rezaei, S. D.; Shannigrahi, S.; Ramakrishna, S. A review of conventional, advanced, and smart glazing technologies and materials for improving indoor environment. *Sol. Energy Mater. Sol. Cells* **2017**, *159*, 26 – 51.

(3) Didier, F.; Jupille, J. Simple views on metal/oxide interfaces: contributions of the long range interactions to the adhesion energy. *J. Adhesion* **1996**, *58*, 253–261.

(4) Cornil, D.; Wiame, H.; Lecomte, B.; Cornil, J.; Beljonne, D. Which oxide for low-emissivity glasses? First-principles modeling of silver adhesion. *ACS Appl. Mater. Interfaces* **2017**, *9*, 18346–18354.

(5) Zúñiga Pérez, J.; Consonni, V.; Lymperakis, L.; Kong, X.; Trampert, A.; Fernández-Garrido, S.; Brandt, O.; Renevier, H.; Keller, S.; Hestroffer, K.

et al. Polarity in GaN and ZnO: Theory, measurement, growth, and devices. *Applied Physics Reviews* **2016**, *3*, 041303.

(6) Goniakowski, J.; Finocchi, F.; Noguera, C. Polarity of oxide surfaces and nanostructures. *Rep. Prog. Phys.* **2008**, *71*, 016501.

(7) Noguera, C.; Goniakowski, J. Polarity in oxide nano-objects. *Chem. Rev.* **2013**, *113*, 4073–4105.

(8) Lin, Z.; Bristowe, P. Microscopic characteristics of the Ag(111)/ZnO(0001) interface present in optical coatings. *Phys. Rev. B* **2007**, *75*, 205423.

(9) Kunat, M.; Girol, S. G.; Becker, T.; Burghaus, U.; Wöll, C. Stability of the polar surfaces of ZnO: A reinvestigation using He-atom scattering. *Phys. Rev. B* **2002**, *66*, 081402R.

(10) Dulub, O.; Diebold, U.; Kresse, G. Novel stabilization mechanism on polar surfaces: ZnO(0001)-Zn. *Phys. Rev. Lett.* **2003**, *90*, 016102.

(11) Kresse, G.; Dulub, O.; Diebold, U. Competing stabilization mechanism for the polar ZnO(0001)-Zn surface. *Phys. Rev. B* **2003**, *68*, 245409.

(12) Meyer, B.; Marx, D. Density-functional study of the structure and stability of ZnO surfaces. *Phys. Rev. B* **2003**, *67*, 035403.

(13) Meyer, B. First-principles study of the polar O-terminated ZnO surface in thermodynamic equilibrium with oxygen and hydrogen. *Phys. Rev. B* **2004**, *69*, 045416.

(14) Du, M. H.; Zhang, S. B.; Northrup, J. E.; Erwin, S. C. Stabilization mechanisms of polar surfaces: ZnO surfaces. *Phys. Rev. B* **2008**, *78*, 155424.

(15) Torbrügge, S.; Ostendorf, F.; Reichling, M. Stabilization of zinc-terminated ZnO(0001) by a modified surface stoichiometry. *J. Phys. Chem. C* **2009**, *113*, 4909–4914.

(16) Valtiner, M.; Todorova, M.; Grundmeier, G.; Neugebauer, J. Temperature stabilized surface reconstructions at polar ZnO(0001). *Phys. Rev. Lett.* **2009**, *103*, 065502.

(17) Lauritsen, J. V.; Porsgaard, S.; Rasmussen, M. K.; Jensen, M. C. R.; Rechstein, R.; Meinander, K.; Clausen, B. S.; Helveg, S.; Wahl, R.; Kresse, G. et al. Stabilization principles for polar surfaces of ZnO. *ACS Nano* **2011**, *5*, 5987–5994.

(18) Wahl, R.; Lauritsen, J. V.; Besenbacher, F.; Kresse, G. Stabilization mechanism for the polar ZnO(000$\bar{1}$)-O surface. *Phys. Rev. B* **2013**, *87*, 085313.

(19) Mora-Fonz, D.; Lazauskas, T.; Farrow, M. R.; Catlow, C. R. A.; Woodley, S. M.; Sokol, A. A. Why are polar surfaces of ZnO stable? *Chem Mater* **2017**, *29*, 5306–5320.

(20) Jedrecy, N.; Renaud, G.; Lazzari, R.; Jupille, J. Flat-top silver nanocrystals on the two polar faces of ZnO: an all angle X-ray scattering investigation. *Phys. Rev. B* **2005**, *72*, 045430.

(21) Jedrecy, N.; Renaud, G.; Lazzari, R.; Jupille, J. Unstrained islands with interface coincidence sites versus strained islands: X-ray measurements on Ag/ZnO. *Phys. Rev. B* **2005**, *72*, 195404.

(22) Ernst, K. H.; Ludviksoson, A.; Zhang, R.; Yoshihara, J.; Campbell, C. T. Growth model for metal films on oxide surfaces: Cu on ZnO(000$\bar{1}$)-O. *Phys. Rev. B* **1993**, *47*, 13782–13796.

(23) Yoshihara, J.; Campbell, J. M.; Campbell, C. T. Cu films on a Zn-terminated ZnO(0001) surface: structure and electronic properties. *Surf. Sci.* **1998**, *406*, 235–245.

(24) Jedrecy, N.; Gallini, S.; Sauvage-Simkin, M.; Pinchaux, R. Copper growth on the O-terminated ZnO(0001)

surface: Structure and morphology. *Phys. Rev. B* **2001**, *64*, 085424.

(25) Koplitz, L. G.; Dulub, O.; Diebold, U. STM Study of copper growth on ZnO(0001)-Zn and ZnO(000$\bar{1}$)-O surfaces. *J. Phys. Chem. B* **2003**, *107*, 10583–10590.

(26) Jacobs, H.; Mokwa, W.; Kohl, D.; Heiland, G. Preparation of Pd/ZnO(000$\bar{1}$) model catalyst and its characterization by AES, LEED and UHV reaction studies. *Surf. Sci.* **1985**, *160*, 217–234.

(27) Petrie, W. T.; Vohs, J. M. Interaction of platinum films with the (000$\bar{1}$) and (0001) surfaces of ZnO. *J. Chem. Phys.* **1994**, *101*, 8098–8107.

(28) Radulovic, P. V.; Feigerle, C. S.; Overbury, S. H. Structure of Pt overlayers on ZnO(0001) and ZnO(000$\bar{1}$) surfaces. *J. Phys. Chem.* **2000**, *104*, 3028–3034.

(29) Vellinga, W. P.; De Hosson, T. M. Atomic structure and orientation relations of the interfaces between Ag and ZnO. *Acta. Mat.* **1997**, *45*, 933–950.

(30) Lazzari, R.; Jupille, J. Growth kinetics and size-dependent wetting of Ag/α-Al$_2$O$_3$(0001) nanoparticles studied via the plasmonic response. *Nanotechnology* **2012**, *23*, 135707.

(31) Lazzari, R.; Renaud, G.; Revenant, C.; Jupille, J.; Borenstzein, Y. Adhesion of growing nanoparticles at a glance: Surface differential reflectivity spectroscopy and grazing incidence small angle X-ray scattering. *Phys. Rev. B* **2009**, *79*, 125428.

(32) Lazzari, R.; Goniakowski, J.; Cabailh, G.; Cavallotti, R.; Trcera, N.; Jupille, J.; Lagarde, P. Surface and epitaxial stress for supported metal clusters. *Nano Lett.* **2016**, *16*, 2574–2579.

(33) Batyrev, E. D.; van den Heuvel, J. C. Modification of the ZnO(0001)-Zn surface under reducing conditions. *Phys. Chem. Chem. Phys.* **2011**, *13*, 13127.

(34) Kroll, M.; Köhler, U. Small Cu-clusters on ZnO(0001)-Zn: Nucleation and annealing behavior. *Surf. Sci.* **2007**, *601*, 2182–2188.

(35) Chernysheva, E.; Srour, W.; Philippe, B.; Baris, B.; Chenot, S.; Duarte, R. F.; Gorgoi, M.; Cruguel, H.; Rensmo, H.; Montigaud, H. et al. Band alignment at Ag/ZnO(0001) interfaces: a combined soft and hard x-ray photoemission study. *Phys. Rev. B* **2018**, *97*, 235430.

(36) Parker, T. M.; Condon, N. G.; Lindsay, R.; Leibsle, F. M.; Thornton, G. Imaging the polar (000$\bar{1}$) and non-polar (10$\bar{1}$0) surfaces of ZnO wih STM. *Surf. Sci.* **1998**, *415*, L1046–L1050.

(37) Dulub, O.; Boatner, L.; Diebold, U. STM study of the geometric and electronic structure of ZnO(0001)-Zn, ZnO(000$\bar{1}$)-O, (10$\bar{1}$0), and(11$\bar{2}$0) surfaces. *Surf. Sci.* **2001**, *519*, 201.

(38) Diebold, U.; Koplitz, L.; Dulub, O. Atomic-scale properties of low-index ZnO surfaces. *Appl. Surf. Sci.* **2004**, *237*, 336–342.

(39) Dulub, O.; Boatneer, L. A.; Diebold, U. STM study of Cu growth on the ZnO(10$\bar{1}$0) surface. *Surf. Sci;* **2002**, *504*, 271–281.

(40) Dulub, O.; Batzill, M.; Diebold, U. Growth of copper on single crystalline ZnO: surface study of a model catalyst. *Top. Catal.* **2005**, *36*, 65–76.

(41) Beinik, I.; Hellström, M.; Jensen, T. N.; Broqvist, P.; Lauritsen, J. V. Enhanced wetting of Cu on ZnO by migration of subsurface oxygen vacancies. *Nat. Commun.* **2015**, *6*, 8845.

(42) Toma, A.; Chiappe, D.; Massabò, D.; Boragno, C.; Buatier de Mongeot, F. Self-organized metal nanowire arrays with tunable optical anisotropy. *Appl. Phys. Lett.* **2008**, *93*, 163104.

(43) Benedetti, S.; Stavale, F.; Valeri, S.; Noguera, C.; Freund, H.-J.; Goniakowski, J.; Nilius, N. Metal nanoparticles: steering the growth of metal adparticles via interface interactions between a MgO thin film and a Mo support. *Adv. Funct. Mater.* **2013**, *23*, 136–136.

(44) Zhang, R.; Bursi, L.; Cox, J. D.; Cui, Y.; Krauter, C. M.; Alabastri, A.; Manjavacas, A.; Calzolari, A.; Corni, S.; Molinari, E. et al. How to identify plasmons from the optical response of nanostructures. *ACS Nano* **2017**, *11*, 7321–7335.

(45) Ma, X.; Dai, Y.; Yu, L.; Bai-Biao, H. Energy transfer in plasmonic photocatalytic composites. *Light: Science and Applications* **2016**, *5*, e16017.

(46) Zapata Herrera, M.; Aizpurua, J.; Kazansky, A. K.; Borisov, A. G. Plasmon response and electron dynamics in charged metallic nanoparticles. *Langmuir* **2016**, *32*, 2829–2840.

(47) Benedetti, S.; Valenti, I.; Valeri, S. Core-shell charge transfer in plasmonic Fe@Ag nanoparticles on MgO Film. *J. Phys. Chem. C* **2019**, *123*, 8206–8211.

(48) Pelli Cresi, J. S.; Spadaro, M. C.; D'Addato, S.; Valeri, S.; Benedetti, S.; Di Bona, A.; Catone, D.; Di Mario, L.; O'Keeffe, P.; Paladini, A. et al. Highly efficient plasmon-mediated electron injection into cerium oxide from embedded silver nanoparticles. *Nanoscale* **2019**, *11*, 10282–10291.

(49) Jiang, D.; Wang, W.; Sun, S.; Zhang, L.; Zheng, Y. Equilibrating the plasmonic and catalytic roles of metallic nanostructures in photocatalytic oxidation over Au-Modified CeO_2. *ACS Catalysis* **2015**, *5*, 613–621.

(50) Horcas, I.; Fernández, R.; Gómez-Rodríguez, J. M.; Colchero, J.; Gómez-Herrero, J.; Baro, A. M. WSXM: A software for scanning probe microscopy and a tool for nanotechnology. *Review of Scientific Instruments* **2007**, *78*, 013705.

(51) Lazzari, R.; Jupille, J.; Cavallotti, R.; Simonsen, I. Model-free unraveling of supported nanoparticles plasmon resonance modes. *J. Phys. Chem. C* **2014**, *118*, 7032–7048.

(52) Lazzari, R.; Roux, S.; Simonsen, I.; Jupille, J.; Bedeaux, D.; Vlieger, J. Multipolar optical absorptions in supported metallic particles: the case of $Ag/Al_2O_3(0001)$. *Phys. Rev. B* **2002**, *65*, 235424–1.

(53) Lazzari, R.; Simonsen, I.; Jupille, J. Onset of charge localisation on coupling multipolar absorption modes in supported silver particles. *Europhys. Lett.* **2003**, *61*, 541–546.

(54) Bedeaux, D.; Vlieger, J. *Optical Properties of Surfaces*; Imperial College Press: London, 2001.

(55) Simonsen, I.; Lazzari, R.; Jupille, J.; Roux, S. Numerical modelling of the optical response of supported metallic particles. *Phys. Rev. B* **2000**, *61*, 7722–7733.

(56) Lazzari, R.; Simonsen, I.; Bedeaux, D.; Vlieger, J.; Jupille, J. Polarizability of truncated spheroidal island supported by a substrate : models and applications. *Eur. Phys. J. B* **2001**, *24*, 267–284.

(57) Lazzari, R.; Simonsen, I. `GranFilm`: a software for calculating thin-layer dielectric properties and Fresnel coefficients. *Thin Solid Films* **2002**, *419*, 124–136.

(58) `GranFilm` can be downloaded with a user guide from: http://www.insp.jussieu.fr/-Logiciels-.html.

(59) Lazzari, R.; Jupille, J. Quantitative analysis of nanoparticle growth through plasmonics. *Nanotechnology* **2011**, *22*, 445703.

(60) Revenant, C.; Renaud, G.; Lazzari, R.; Jupille, J. Defect-pinned nucleation, growth, and dynamic coalescence of Ag islands on MgO(001): an *in situ* grazing-incidence small-angle X-ray scattering study. *Phys. Rev. B* **2009**, *79*, 235424.

(61) Giannozzi, P.; Andreussi, O.; Brumme, T.; Bunau, O.; Buongiorno Nardelli, M.; Calandra, M.; Car, R.; Cavazzoni, C.; Ceresoli, D.; Cococcioni, M. et al. Advanced capabilities for materials modelling with Quantum ESPRESSO. *J. Phys.: Condens. Matter* **2017**, *29*, 465901.

(62) Perdew, J. P.; Burke, K.; Ernzerhof, M. Generalized Gradient Approximation made simple. *Phys. Rev. Lett.* **1996**, *77*, 3865–3868.

(63) Tasker, P. W.; Duffy, D. M. The structure and properties of the stepped surfaces of MgO and NiO. *Surf. Sci.* **1984**, *137*, 91–02.

(64) Finocchi, F.; Geysermans, P.; Bourgeois, A. The role of hydroxylation in the step stability and in the interaction between steps: a first-principles study of vicinal MgO surfaces. *Phys. Chem. Chem. Phys.* **2012**, *14*, 13692–13701.

(65) Kroll, M.; Kuschel, T.; Löber, T.; Köhler, U. Large scale morphology of ZnO(10$\bar{1}$0)-surfaces. *Surf. Sci.* **2009**, *603*, L49 – L51.

(66) Ozawa, K.; Sato, T.; Kato, M.; Edamoto, K.; Aiura, Y. Angle-resolved photoemission spectroscopy study of adsorption process and electronic structure of silver on ZnO(10$\bar{1}$0). *J. Phys. Chem. B* **2005**, *109*, 14619–14626.

(67) Lüth, H. *Surface and Interfaces of Solids*; Springer Study Edition; Springer-Verlag Berlin Heidelberg, 1992.

(68) Lazzari, R.; Jupille, J. Silver layers on oxide surfaces: morphology and optical properties. *Surf. Sci.* **2001**, *482-485*, 823–827.

(69) Lazzari, R.; Jupille, J. Interfacial chemistry and wetting of metallic films on the hydroxylated α-Al$_2$O$_3$(0001) surface. *Phys. Rev. B* **2005**, *71*, 045409.

(70) Jellison, G. E.; Batner, L. A. Optical functions of uniaxial ZnO determined by generalized ellipsometry. *Phys. Rev. B* **1998**, *58*, 3586–3589.

(71) Yamaguchi, T.; Yoshida, S.; Kinbara, A. Anomalous optical absorption of aggregated silver films. *Thin Solid Films* **1973**, *18*, 63–70.

(72) Lazzari, R. Vers la maîtrise de la croissance des couches minces: une étude par spectroscopie optique et d'électrons. Ph.D. thesis, Université Paris XI, France, 2000.

(73) Lazzari, R.; Simonsen, I.; Jupille, J. Interfacial susceptibilities in nanoplasmonics via inversion of Fresnel coefficients. *Plasmonics* **2014**, *9*, 261–272.

(74) Palik, E. D. *Handbook of Optical Constants of Solids*; Academic Press, 1985; Vol. 1-3.

Graphical TOC Entry

Ag@ZnO polar step